

Interference effects and the use of Higgs boson pair production to study the Higgs trilinear self coupling

Duane A. Dicus,^{1,*} Chung Kao,^{2,†} and Wayne W. Repko^{3,‡}

¹*Center for Particle Physics, University of Texas, Austin, TX 78712, USA*

²*Homer L. Dodge Department of Physics, University of Oklahoma, Norman, OK 73019, USA*

³*Department of Physics and Astronomy, Michigan State University, East Lansing, MI 48824, USA*

(Dated: November 10, 2021)

We show that the dominant channel proposed for the determination of the Higgs boson trilinear coupling, $pp \rightarrow HH + X$ via gluon fusion, exhibits an interference structure that is independent of the collider energy for collider energies in the range $8 \text{ TeV} \leq \sqrt{s} \leq 100 \text{ TeV}$ and is almost maximally destructive. This insensitivity to the collider energy remains approximately true for a variety of other two Higgs production mechanisms although the magnitude of the interference varies widely.

PACS numbers: 13.38.Dg

1. INTRODUCTION

The standard Higgs self interaction is contained in the Higgs potential

$$V(H) = \lambda v^2 H^2 + \lambda v H^3 + \frac{1}{4} \lambda H^4, \quad (1)$$

where $\lambda = m_H^2/2v^2$ and, in terms of the W mass, the weak mixing angle and the fine structure constant, $v = M_W \sin \theta_W / \sqrt{\pi \alpha}$. A measurement of the trilinear coupling is an important test of the Standard model behavior of the Higgs-like object discovered at the LHC [1, 2]. Given the proliferation of gluon production at the Large Hadron Collider, the natural choice for the study of the Higgs boson trilinear coupling is the gluon fusion process $gg \rightarrow HH$ [3–13]. The matrix element comes from the sum of a triangle graph and several box graphs as indicated in Fig. 1. Each of these two contributions is gauge invariant. By calculating the total cross section,



FIG. 1: The leading order triangle and a representative box diagram are shown.

σ_{TOT} and separately calculating the cross sections from just triangle graph, σ_T , and just the box graphs, σ_B , we can study the interference between the two amplitudes. Defining interference angle α_I by the equation

$$\sigma_{TOT} = \sigma_T + \sigma_B + 2 \cos(\alpha_I) \sqrt{\sigma_T \sigma_B}, \quad (2)$$

we can examine how $\cos(\alpha_I)$ varies as a function of energy. Since the interference term between the box and triangle amplitudes is $2 \Re(\mathcal{M}_B \mathcal{M}_T^*) = 2 |\mathcal{M}_B| |\mathcal{M}_T| \cos(\alpha_I)$, $\cos(\alpha_I)$ is independent of the three Higgs boson self coupling.

*Electronic address: dicus@physics.utexas.edu

†Electronic address: kao@physics.ou.edu

‡Electronic address: repko@pa.msu.edu

2. RESULTS FOR $gg \rightarrow HH$

The numerical results that are shown in Table I were obtained using $M_H = 125.5$ GeV, $M_t = 173.1$ GeV and the MSTW2008 [14] parton distribution functions (PDFs) with both scales equal to the invariant mass of the two Higgs final state. The leading-order amplitudes for Higgs pair production from gluon fusion can be expressed in terms of tensor integrals [15] and scalar integrals [16]. We evaluate these integrals numerically with a FORTRAN code [17] developed for this purpose. The cross section was calculated in the usual way and then Eq. (2) was used to find $\cos(\alpha_I)$. The error in these values of $\cos(\alpha_I)$ from the numerical integration varies from 0.005 at low energies to 0.01 at high energies. The negative value of $\cos(\alpha_I)$ reflects the known fact that the interference

\sqrt{s} (TeV)	$\sigma_B(fb)$	$\sigma_T(fb)$	$\sigma_{TOT}(fb)$	$\cos(\alpha_I)$
8	9.06	1.34	4.11	-0.902
13	31.6	4.36	14.9	-0.898
14	37.8	5.16	17.9	-0.898
33	243.	30.3	120.	-0.893
60	760.	89.8	383.	-0.893
100	1900.	212.	965.	-0.904

TABLE I: For $pp \rightarrow HH + X$ from $gg \rightarrow HH$, the center of mass energy, the LO contributions to the cross section from the box, the triangle, and the total cross section, and $\cos(\alpha_I)$.

is destructive. What is surprising is that $\cos(\alpha_I)$ is almost universal.

To check the numbers in Table I, we multiply the total cross section, σ_{TOT} , by the K factor given by de Florian and Mazzitelli [12]

$$K = 1.242 - 7.17 \left(\frac{E}{1 \text{ TeV}} \right)^{-1} + 5.77 \left(\frac{E}{1 \text{ TeV}} \right)^{-1/2}, \quad (3)$$

where E is the center of mass energy. This reproduces their NNLO numbers precisely.

Since it is not clear how $\cos(\alpha_I)$ can be so constant with energy, it makes sense to ask how it varies with other factors. It is well known that the process, $gg \rightarrow HH$ is very sensitive to the values of the scales and the PDFs. To see how $\cos(\alpha_I)$ depends on the scales and PDF we give in Table II the box contribution, triangle contribution, total cross section, and $\cos(\alpha_I)$ for three combinations of scale and PDF at three energies. For each energy the first line is the MSTW PDF with the scales equal to the two Higgs invariant mass (same as Table I). The second line uses the CTEQ6L1 PDF [18] with the same scales, and the third line uses the MSTW PDF but with the scales equal to M_H . Again the cross sections were calculated from the matrix elements and then $\cos(\alpha_I)$ was determined from Eq. (2).

\sqrt{s} (TeV)	$\sigma_B(fb)$	$\sigma_T(fb)$	$\sigma_{TOT}(fb)$	$\cos(\alpha_I)$
8	9.06	1.34	4.11	-0.903
	8.05	1.20	3.64	-0.902
14	15.3	2.06	7.32	-0.894
	37.8	5.16	17.9	-0.897
	35.0	4.79	16.5	-0.899
100	60.5	7.53	29.9	-0.893
	1900.	212.	965.	-0.904
	1790.	198.	914.	-0.902
	2530.	266.	1340.	-0.887

TABLE II: For the cross sections of $pp \rightarrow HH + X$ from $gg \rightarrow HH$ the dependence of $\cos(\alpha_I)$ on the PDF (first and second line at each energy) or on the scale (first and third line at each energy).

These results are very striking because, as can be seen, the contributions to the triangle and box cross sections and the total cross section are very dependent on the scales and somewhat dependent on the PDF. But $\cos(\alpha_I)$ apparently doesn't care about such things.

To separate the effects of the underlying physics from that of the parton distribution functions, consider the contributions with the distribution functions set to unity, effectively examining the behavior of the partonic

process. Here we have to consider smaller energies because the triangle graph gets small rapidly due to the s-channel pole. The results are shown in Table III.

$\sqrt{\hat{s}}$ (GeV)	$\hat{\sigma}_B(fb)$	$\hat{\sigma}_T(fb)$	$\hat{\sigma}_{TOT}(fb)$	$\cos(\alpha_I)$
300	0.199	0.682×10^{-1}	0.342×10^{-1}	-1.00
400	0.964	0.875×10^{-1}	0.482	-0.980
500	0.900	0.497×10^{-1}	0.552	-0.940
1000	0.199	0.277×10^{-2}	0.165	-0.783
2000	0.447×10^{-1}	0.995×10^{-4}	0.425×10^{-1}	-0.545
4000	0.114×10^{-1}	0.303×10^{-5}	0.113×10^{-1}	-0.277

TABLE III: The cross sections and $\cos(\alpha_I)$ with the distribution functions are set to one, i.e., the parton cross sections $\hat{\sigma}(gg \rightarrow HH)$ are shown.

The last two lines are uncertain because they depend on the σ_B and σ_{TOT} being very accurate. However, the conclusion is clear; without the distribution functions to emphasize the low energy parts of the cross sections, $\cos(\alpha_I)$ is no longer universal. More specifically, this Table shows that the behavior of the partonic cross section near threshold ($\sqrt{\hat{s}} \sim 300 - 500$ GeV) deduced in [19, 20] using unitarity cutting rules is the basically the only region probed by the full cross section $\sigma(pp \rightarrow HH + X)$ no matter what the center of mass energy happens to be.

3. INTERFERENCE IN OTHER TWO HIGGS PROCESSES

3.1. Production of two Higgs in association with a Z or W

It is worth looking at other two Higgs production processes to see how $\cos(\alpha_I)$ varies with energy for them. We call the background, B , the contribution from the diagrams where both Higgs are emitted separately from the Z line. The signal is the contribution from the diagram with the three Higgs coupling. In analogy to the gluon fusion case above, we call that T . The total cross section is the square of all the diagrams including the cross terms between the B part and the T part. $\cos(\alpha_I)$ is then defined by Eq. (2) above. First consider the results for $pp \rightarrow ZHH + X$ shown in Table IV for the same energies used in Table I.

$\sqrt{\hat{s}}$ (TeV)	σ_B	σ_T	σ_{TOT}	$\cos(\alpha_I)$
8	5.37×10^{-2}	9.10×10^{-3}	9.38×10^{-2}	0.701
13	0.135	2.21×10^{-2}	0.229	0.658
14	0.153	2.51×10^{-2}	0.260	0.661
33	0.588	9.31×10^{-2}	0.975	0.628
60	1.34	0.212	2.23	0.636
100	2.67	0.411	4.34	0.601

TABLE IV: Cross sections and interference for $pp \rightarrow ZHH + X$. The cross sections are in fb. The different contributions again refer to Eq. (2) above. The error in $\cos(\alpha_I)$ due to roundoff is less than or equal to 0.01.

We see that $\cos(\alpha_I)$ changes only from 0.7 to 0.6 so unlike gluon production of two Higgs it does change but it doesn't change much. For this reaction and the remaining reactions, the CTEQ6L1 distribution functions were used with scale equal to $\sqrt{\hat{s}}$. We did try varying the distribution functions and found that it makes very little difference which set of PDF's is used. The scale used makes large differences in the values of cross sections but, for a given energy, they all change in the same way so $\cos(\alpha_I)$ is unchanged.

The processes $pp \rightarrow W^\pm HH + X$ have an interference behavior similar to $pp \rightarrow ZHH + X$. For the same range of energies, $\cos(\alpha_I)$ changes from 0.66 at 8 TeV to 0.57 at 100 TeV for W^+ and 0.69 to 0.58 for W^- . The results are shown in Tables V and VI.

For $p\bar{p} \rightarrow ZHH$, rather than $pp \rightarrow ZHH + X$ as given above, $\cos(\alpha_I)$, shown in Table VII, is 0.63 at 8 TeV and 0.60 at 100 TeV. So the change in the interference with energy when using two quark distributions is even less than when using one quark and one antiquark.

\sqrt{s} (TeV)	σ_B	σ_T	σ_{TOT}	$\cos(\alpha_I)$
8	5.81×10^{-2}	1.15×10^{-2}	0.104	0.665
13	0.136	2.61×10^{-2}	0.237	0.629
14	0.153	2.92×10^{-2}	0.266	0.627
33	0.543	0.101	0.923	0.596
60	1.21	0.221	2.03	0.579
100	2.31	0.418	3.85	0.571

TABLE V: Cross sections and interference for $pp \rightarrow W^+ HH + X$. The cross sections are in fb.

\sqrt{s} (TeV)	σ_B	σ_T	σ_{TOT}	$\cos(\alpha_I)$
8	2.54×10^{-2}	5.10×10^{-3}	4.63×10^{-2}	0.694
13	6.84×10^{-2}	1.35×10^{-2}	0.122	0.660
14	7.86×10^{-2}	1.54×10^{-2}	0.139	0.647
33	0.333	6.28×10^{-2}	0.573	0.613
60	0.807	0.150	1.37	0.594
100	1.64	0.300	2.76	0.585

TABLE VI: Cross sections and interference for $pp \rightarrow W^- HH + X$. The cross sections are in fb.

\sqrt{s} (TeV)	σ_B	σ_T	σ_{TOT}	$\cos(\alpha_I)$
8	0.104	1.66×10^{-2}	0.173	0.631
14	0.217	3.40×10^{-2}	0.360	0.634
33	0.657	0.102	1.07	0.601
60	1.42	0.219	2.31	0.602
100	2.72	0.417	4.41	0.598

TABLE VII: Cross section and interference for $p\bar{p} \rightarrow ZHH$. The cross sections are in fb.

3.2. Production of two Higgs in association with a $t\bar{t}$ pair

Another reaction for producing two Higgs is $pp \rightarrow t\bar{t}HH + X$. This has contributions from initial quarks and from initial gluons which can not be separated experimentally. But they must be calculated separately so let us first consider the $q\bar{q} \rightarrow t\bar{t}HH$ part. For all the same input parameters, distribution functions, and scales as above our results are shown in Table VIII. Here, $\cos(\alpha_I)$ varies only from 0.84 to 0.76 over the usual enormous energy range. The other contribution to $pp \rightarrow t\bar{t}HH + X$ is from $gg \rightarrow t\bar{t}HH$. The results are shown in Table IX. Of course we can't measure the quark and gluon processes separately. If we ignore the fact that the K factors

\sqrt{s} (TeV)	σ_B	σ_T	σ_{TOT}	$\cos(\alpha_I)$
8	6.47×10^{-2}	1.96×10^{-3}	8.56×10^{-2}	0.841
13	0.212	6.54×10^{-3}	0.280	0.825
14	0.249	7.68×10^{-3}	0.328	0.815
33	1.19	3.75×10^{-2}	1.56	0.788
60	2.98	9.51×10^{-2}	3.89	0.765
100	6.15	0.197	8.04	0.769

TABLE VIII: Contributions to the cross section $pp \rightarrow t\bar{t}HH + X$ from $q\bar{q} \rightarrow t\bar{t}HH$. As always the cross sections are in fb.

would be different and just add these last two LO processes to get a total cross section for $pp \rightarrow t\bar{t}HH + X$ we get the result shown in Table X. Finally we have a process where $\cos(\alpha_I)$ varies substantially with the energy.

\sqrt{s} (TeV)	σ_B	σ_T	σ_{TOT}	$\cos(\alpha_I)$
8	2.79×10^{-2}	1.40×10^{-3}	3.28×10^{-2}	0.280
13	0.179	1.03×10^{-2}	0.211	0.253
14	0.231	1.36×10^{-2}	0.273	0.253
33	2.93	0.205	3.47	0.216
60	12.6	0.966	15.0	0.206
100	38.2	3.11	45.5	0.192

TABLE IX: Contributions to the cross section $pp \rightarrow t\bar{t}HH + X$ from initial gluons.

\sqrt{s} (TeV)	σ_B	σ_T	σ_{TOT}	$\cos(\alpha_I)$
8	9.26×10^{-2}	3.36×10^{-3}	0.120	0.681
13	0.391	1.68×10^{-2}	0.491	0.513
14	0.480	2.12×10^{-2}	0.600	0.490
33	4.12	0.243	5.03	0.333
60	15.6	1.06	18.9	0.275
100	44.4	3.31	53.6	0.243

TABLE X: Contributions to the cross sections and interference for the total process $pp \rightarrow t\bar{t}HH + X$.

3.3. HH production from $qq \rightarrow qqHH$

The results for $pp \rightarrow qqHH$ via the subprocesses $uu \rightarrow uuHH$, $dd \rightarrow ddHH$ and $ud \rightarrow udHH$ are shown in Tables XI, XII and XIII. Again, there is very little spread the values of $\cos(\alpha_I)$ but the interference is, like $gg \rightarrow HH$, destructive.

\sqrt{s} (TeV)	σ_B	σ_T	σ_{TOT}	$\cos(\alpha_I)$
8	5.87×10^{-2}	1.53×10^{-2}	2.30×10^{-2}	-0.846
13	0.161	3.81×10^{-2}	6.90×10^{-2}	-0.830
14	0.185	4.32×10^{-2}	8.43×10^{-2}	-0.805
33	0.766	0.157	0.376	-0.789
60	1.80	0.341	0.938	-0.768
100	3.55	0.638	1.91	-0.757

TABLE XI: Contribution to the cross section $pp \rightarrow uuHH + X$ from the subprocess $uu \rightarrow uuHH$. Again all cross sections are in fb and the errors in $\cos(\alpha_I)$ are less than or equal to 0.01.

\sqrt{s} (TeV)	σ_B	σ_T	σ_{TOT}	$\cos(\alpha_I)$
8	2.10×10^{-2}	5.80×10^{-3}	7.80×10^{-3}	-0.861
13	6.65×10^{-2}	1.69×10^{-2}	2.69×10^{-2}	-0.843
14	7.81×10^{-2}	1.96×10^{-2}	3.20×10^{-2}	-0.840
33	0.404	8.95×10^{-2}	0.186	-0.809
60	1.08	0.224	0.531	-0.786
100	2.36	0.464	1.20	-0.776

TABLE XII: Contribution to the cross section $pp \rightarrow ddHH + X$ from the subprocess $dd \rightarrow ddHH$.

3.4. HH production from $q\bar{q} \rightarrow q\bar{q}HH$

The contributions from the subprocesses $u\bar{u} \rightarrow u\bar{u}HH$ and $d\bar{d} \rightarrow d\bar{d}HH$ are shown in Tables XIV and XV.

\sqrt{s} (TeV)	σ_B	σ_T	σ_{TOT}	$\cos(\alpha_I)$
8	0.404	0.128	0.141	-0.860
13	1.18	0.344	0.452	-0.841
14	1.36	0.394	0.530	-0.836
33	6.24	1.60	2.76	-0.804
60	15.6	3.72	7.32	-0.788
100	32.2	7.36	15.8	-0.772

TABLE XIII: Contribution to the cross section $pp \rightarrow udHH + X$ from the subprocess $ud \rightarrow udHH$.

\sqrt{s} (TeV)	σ_B	σ_T	σ_{TOT}	$\cos(\alpha_I)$
8	1.46×10^{-2}	3.82×10^{-3}	9.58×10^{-3}	-0.592
13	5.03×10^{-2}	1.27×10^{-2}	2.92×10^{-2}	-0.669
14	6.00×10^{-2}	1.50×10^{-2}	3.44×10^{-2}	-0.677
33	0.366	8.36×10^{-2}	0.196	-0.725
60	1.08	0.231	0.577	-0.735
100	2.52	0.512	1.36	-0.736

TABLE XIV: Contribution to the cross section $pp \rightarrow u\bar{u}HH + X$ from the subprocess $u\bar{u} \rightarrow u\bar{u}HH$.

\sqrt{s} (TeV)	σ_B	σ_T	σ_{TOT}	$\cos(\alpha_I)$
8	1.33×10^{-2}	3.56×10^{-3}	8.95×10^{-3}	-0.575
13	4.74×10^{-2}	1.21×10^{-2}	2.79×10^{-2}	-0.660
14	5.67×10^{-2}	1.49×10^{-2}	3.30×10^{-2}	-0.664
33	0.359	8.30×10^{-2}	0.193	-0.721
60	1.10	0.238	0.590	-0.731
100	2.61	0.538	1.41	-0.733

TABLE XV: Contribution to the cross section $pp \rightarrow d\bar{d}HH + X$ from the subprocess $d\bar{d} \rightarrow d\bar{d}HH$.

4. CONCLUSIONS

As discussed in the Introduction, the interference, as parameterized by $\cos(\alpha_I)$, does not depend on the value of the Higgs coupling. For two Higgs production the interference between the graphs with the trilinear coupling and those without is usually constructive. In the exceptional cases of $gg \rightarrow HH$ and $qq \rightarrow qqHH$ the interference is strongly destructive. For all cases the approximate constancy of $\cos(\alpha_I)$ is a result of the near threshold behavior of the amplitudes and the large values of the parton luminosity in the threshold region. For the dominant subprocess, $gg \rightarrow HH$, the almost maximal destructive interference between the triangle and box amplitudes ($\cos(\alpha_I) = -0.90$) obtained using unitarity cutting [19, 20] tends to make the total cross section small and thus difficult to measure.

We note that $pp \rightarrow t\bar{t}HH + X$ has constructive interference between diagrams with trilinear Higgs couplings and those without, and the interference angle $\cos(\alpha_I)$ depends on the collider energy as demonstrated in Table X. For collider energy less than 14 TeV, quark-antiquark fusion is the dominant source of $t\bar{t}HH$, while gluon fusion makes larger contribution for collider energy greater than 33 TeV. Thus parton distribution functions enhance the threshold effect of $q\bar{q} \rightarrow t\bar{t}HH$ ($\sqrt{s} \leq 14$ TeV) and $gg \rightarrow t\bar{t}HH$ ($\sqrt{s} \geq 33$ TeV) in $pp \rightarrow t\bar{t}HH + X$ at different values of collider energy.

For all the processes, except $gg \rightarrow HH$, unitarity arguments are not of use since the leading amplitudes occur at the tree level. Nevertheless, these partonic amplitudes lead to a similar maximal interference in the hadronic cross sections near threshold. As can be seen in Tables XVI and XVII for $u\bar{u} \rightarrow ZHH$ and $u\bar{u} \rightarrow t\bar{t}HH$, the maximal interference region is not quite as persistent as in the dominant $gg \rightarrow HH$ case so the integration over the relevant parton luminosities results in a clustering of the interference terms rather than yielding a constant value.

If we allow the standard model Higgs trilinear coupling to vary by a factor κ ($\kappa\lambda v H^3$ in Eq. (1)), the results for $gg \rightarrow HH$ are illustrated in Fig. 2. In addition, Fig. 3 shows that $\cos(\alpha_I)$ remains constant for any κ .

$\sqrt{\hat{s}}$ (GeV)	$\hat{\sigma}_B(fb)$	$\hat{\sigma}_T(fb)$	$\hat{\sigma}_{TOT}(fb)$	$\cos(\alpha_I)$
350	0.453×10^{-3}	0.126×10^{-3}	0.106×10^{-2}	0.999
400	0.122×10^{-1}	0.277×10^{-2}	0.262×10^{-1}	0.964
500	0.312×10^{-1}	0.571×10^{-2}	0.589×10^{-1}	0.821
1000	0.335×10^{-1}	0.416×10^{-2}	0.453×10^{-1}	0.325
2000	0.181×10^{-1}	0.148×10^{-2}	0.207×10^{-1}	0.106
4000	0.794×10^{-2}	0.421×10^{-3}	0.849×10^{-2}	0.0337

TABLE XVI: To separate the effect of the distribution functions we show the partonic cross sections $\hat{\sigma}(u\bar{u} \rightarrow ZHH)$ along with $\cos(\alpha_I)$ as a function of $\sqrt{\hat{s}}$.

$\sqrt{\hat{s}}$ (GeV)	$\hat{\sigma}_B(fb)$	$\hat{\sigma}_T(fb)$	$\hat{\sigma}_{TOT}(fb)$	$\cos(\alpha_I)$
600	0.469×10^{-6}	0.126154×10^{-7}	0.655×10^{-6}	1.000
700	0.340×10^{-1}	0.101×10^{-2}	0.464×10^{-1}	0.975
800	0.119	0.343×10^{-2}	0.160	0.933
900	0.189	0.548×10^{-2}	0.251	0.890
1000	0.229	0.676×10^{-2}	0.302	0.849
1500	0.212	0.714×10^{-2}	0.273	0.690
2000	0.146	0.552×10^{-2}	0.185	0.588

TABLE XVII: Same as Table XVI for $\hat{\sigma}(u\bar{u} \rightarrow t\bar{t}HH)$.

A summary of the results for $\cos(\alpha_I)$ given in the Tables is shown in Fig.4 which illustrates again that, while the value of the interference is very different for different processes, there is very little variation with energy within a given process.

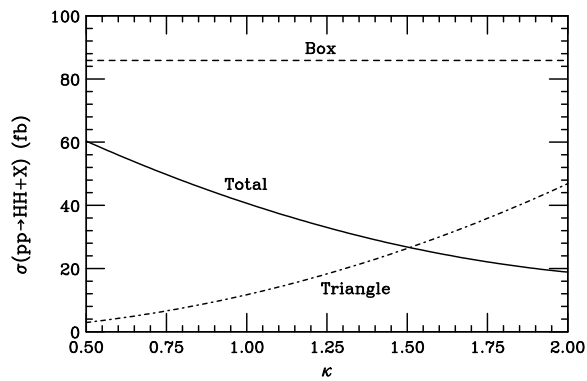


FIG. 2: The dependence of the $pp \rightarrow HH + X$ cross section from the subprocess $gg \rightarrow HH$ as a function of the ratio of the trilinear coupling to the Standard model coupling is illustrated for $\sqrt{s} = 14$ TeV and the 2.27 K -factor from Eq. (3).

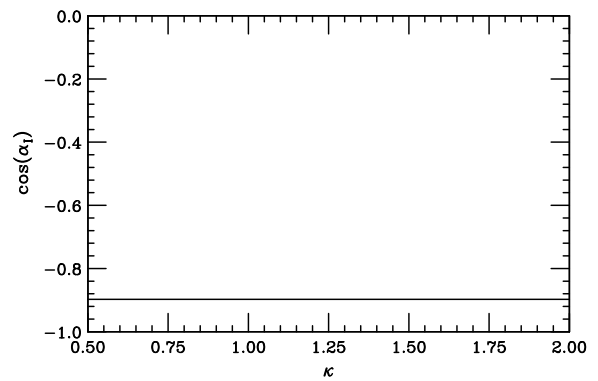


FIG. 3: The invariance of $\cos(\alpha_I)$ for changes in the trilinear couplings is shown for the particular case of $\sqrt{s} = 14$ TeV and the 2.27 K -factor from Eq. (3).

Acknowledgements

D. A. D. was supported in part by the U. S. Department of Energy under Award No.DE-FG02-12ER41830, C. K. was supported in part by the U. S. Department of Energy under Award No.DE-FG02-13ER41979 and W. W. R. was supported in part by the National Science Foundation under Grant No. PHY 1068020.

-
- [1] ATLAS Collaboration, Phys. Lett. B **716**, 1 (2012).
 [2] CMS Collaboration, Phys. Lett. B **716**, 30 (2012).
 [3] T. Binoth, S. Karg, N. Kauer and R. Ruckl, Phys. Rev. D **74**, 113008 (2006) [hep-ph/0608057].
 [4] M. J. Dolan, C. Englert and M. Spannowsky, JHEP **1210**, 112 (2012) [arXiv:1206.5001 [hep-ph]].
 [5] J. Baglio, A. Djouadi, R. Grber, M. M. Mhleitner, J. Quevillon and M. Spira, JHEP **1304**, 151 (2013) [arXiv:1212.5581 [hep-ph]].
 [6] F. Goertz, A. Papaefstathiou, L. L. Yang and J. Zurita, JHEP **1306**, 016 (2013) [arXiv:1301.3492 [hep-ph]].
 [7] A. J. Barr, M. J. Dolan, C. Englert, D. E. F. de Lima and M. Spannowsky, arXiv:1412.7154 [hep-ph].
 [8] A. Arhrib, R. Benbrik, C. H. Chen, R. Guedes and R. Santos, JHEP **0908**, 035 (2009) [arXiv:0906.0387 [hep-ph]].
 [9] D. de Florian and J. Mazzitelli, Phys. Lett. B **724**, 306 (2013) [arXiv:1305.5206 [hep-ph]].
 [10] B. Hespel, D. Lopez-Val and E. Vryonidou, JHEP **1409**, 124 (2014) [arXiv:1407.0281 [hep-ph]].
 [11] N. Liu, S. Hu, B. Yang and J. Han, JHEP **1501**, 008 (2015) [arXiv:1408.4191 [hep-ph]].
 [12] D. de Florian and J. Mazzitelli, Phys. Rev. Lett. **111**, 201801 (2013).
 [13] R. Frederix, S. Frixione, V. Hirschi, F. Maltoni, O. Mattelaer, P. Torrielli, E. Vryonidou and M. Zaro, Phys. Lett. B **732**, 142 (2014) [arXiv:1401.7340 [hep-ph]].
 [14] A. D. Martin, W. J. Stirling, R. S. Thorne and G. Watt, Eur. Phys. J. C **63**, 189 (2009), A. D. Martin, W. J. Stirling, R. S. Thorne and G. Watt, Eur. Phys. J. C **64**, 653 (2009).
 [15] G. Passarino and M. Veltman, Nucl. Phys. **B160**, 151 (1979).
 [16] G. 't Hooft and M. Veltman, Nucl. Phys. **B153**, 365 (1979).
 [17] C. Kao and D. A. Dicus, LOOP, a FORTRAN program for evaluating loop integrals based on the results in Refs. [15] and [16].
 [18] P. Nadolsky, *et. al*, Phys. Rev. D **78**, 013004 (2008).
 [19] For a detailed discussion of the analytic properties of the $gg \rightarrow HH$ partonic amplitudes, see: X. Li and M. B. Voloshin, Phys. Rev. D **89**, 013012 (2014).
 [20] S. Dawson, A. Ismail and I. Low, Phys. Rev. D **91**, no. 11, 115008 (2015) [arXiv:1504.05596 [hep-ph]].

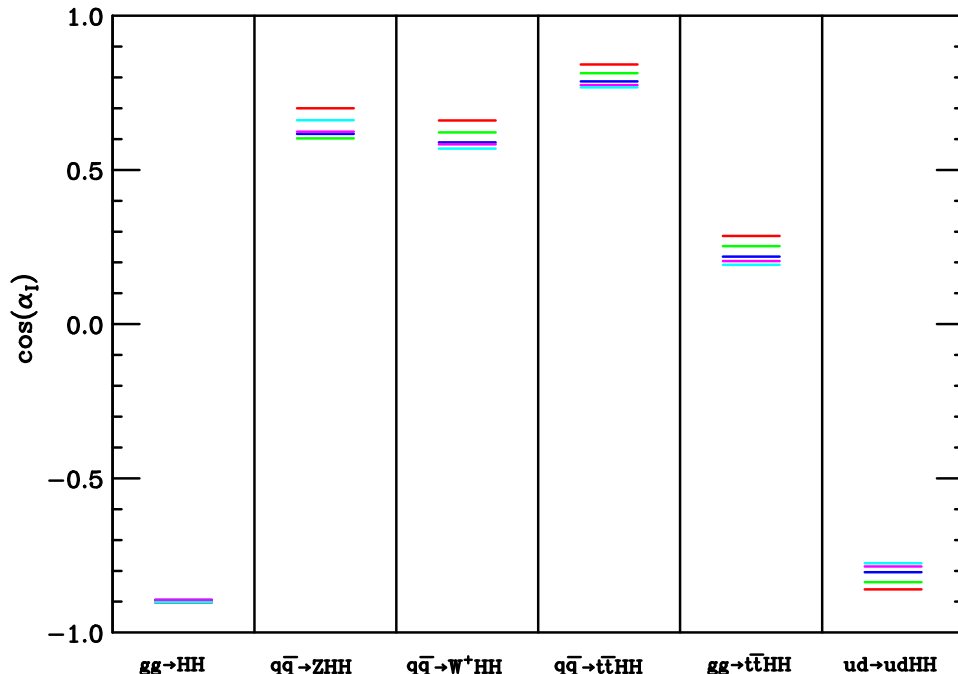


FIG. 4: The values of $\cos(\alpha_1)$ are plotted. Note that each partonic initial state has been integrated over the appropriate parton distribution functions for pp collisions. For each process the different lines are for different energies ranging from 8 TeV for the line with the largest magnitude to 100 TeV for the line with the smallest magnitude.